HERIOT-WATT
UNIVERSITY
Edinburgh

Topographical Measurements of Water Waves at a Matrix of Measuring Points

Project Work by
Peter Vennemann
at the
Fluid Loading and Instrumentation Centre
Professor Ian Grant
Supervisor: Dr. Hannes Reinecke

DEPARTMENT OF
CIVIL AND OFFSHORE ENGINEERING

This study was done in the scope of the SOCRATES-ERASMUS Programme of the European Union in co-operation of

Fluid Loading and Instrumentation Centre
Professor Ian Grant

and

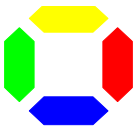

Universität Essen
Lehrstuhl für Strömungslehre
Prof. Dr. rer. nat. Wolfgang Merzkirch

Acknowledgements

I thank Prof. Dr. rer. nat. Wolfgang Merzkirch and Prof. Ian Grant for enabling me to do this project work from April 2000 to October 2000 as an ERASMUS exchange student at the Heriot-Watt University in Edinburgh, Scotland.

I also thank my supervisor Hannes Reinecke for his instructions, his help and advice.

Further I want to thank the postgraduate student Min-Gan Mo and the PhD student Vladimir Fonov for their support and my fellow student Marco Wildemann, who worked at the same project, for his cooperation.

After all I thank my girlfriend Margret Volkenhoff for visiting me in Edinburgh and for reading and correcting this work.

Table of Contents

1 Introduction

1.1 Necessity of Measuring the Shape of a Water Wave

The measurement of the shape of a water wave is important for the study of a wide range of questions like the understanding of wave motions, the wave shapes dependence on the quality of the ground, the water depth or the surface tension which might be altered by pollution. The mixing of substances or gases at the surface of the sea is dependent on the waves shapes. The shape of a water wave is also interesting for understanding the transport mechanisms and the energy of waves. Knowledge about water wave shapes is essential for the design of an effective shore protection which is going to be more and more important when the sea level is rising. Furthermore offshore designers require knowledge about the shape of a wave during its interaction with installations for optimising the shape of offshore structures and for calculating the loading. This is a key requisite for the design and the construction of cost effective and save structures of any kind like buoys, lifeboats, ships, oil rigs or other offshore platforms. Measurements of wave shapes for example can help to understand the interference or upwelling caused by the legs of typical offshore platform geometries which can enhance the wave amplitude and possible wave impact with the underside of the platform.

1.2 Measuring Methods

The probably simplest way of measuring the surface of a wave is to put a certain number of water depth gauges into the water, taking a photo of the wave when it is passing the gauges and then reading every single measure from the photograph. The wave shape can be reconstructed by interpolating the waves surface between the measuring points. The considerable distortion of the measuring object by the measuring instruments is disadvantageous.

An array of pressure sensors in a plain below the water surface can be used instead of the gauges to avoid the distortions. The pressure at every single sensor is a measure for the water height above the sensor. The disadvantage of this method is the sensitivity of the pressure sensors for the dynamic pressure of water flows caused by turbulences, in particular in shallow water, underneath breaking waves or

close to constructions. Also disadvantageous is the necessity of mounting a part of the measuring system under the water.

To avoid this problems, photographic methods for the recording of surface waves have been developed:

At the beginning of the 20th century the first attempts have been made to collect elevation data of ocean waves by stereo photography. Referring to [1, Holthuijsen 1993] the principle of stereo-photography is taking two pictures of the same object from different viewpoints. Afterwards unique points are identified on both pictures. From the two dimensional coordinates in the photographs the three dimensional coordinates of these points can be calculated in a reference coordinate system. Figure 1.1 illustrates the principle. The small grey squares symbolise the two pictures with the distance b from midpoint to midpoint. Holthuijsen calculates the coordinates of the point $(x,y,z)^T$ as follows: $x=(b\cdot x_1)/(x_1-x_2)$, $y=(b\cdot y)/(x_1-x_2)$ and $z=h-(b\cdot f)/(x_1-x_2)$.

The water surface need to be marked with dots or identifiable structures for using stereo photography. A difficulty is to determine which points on the two pictures correspond to the same point on the object. [2, Shemdin 1990] explains accurate and cost effective, automatic digital stereo-correlation techniques.

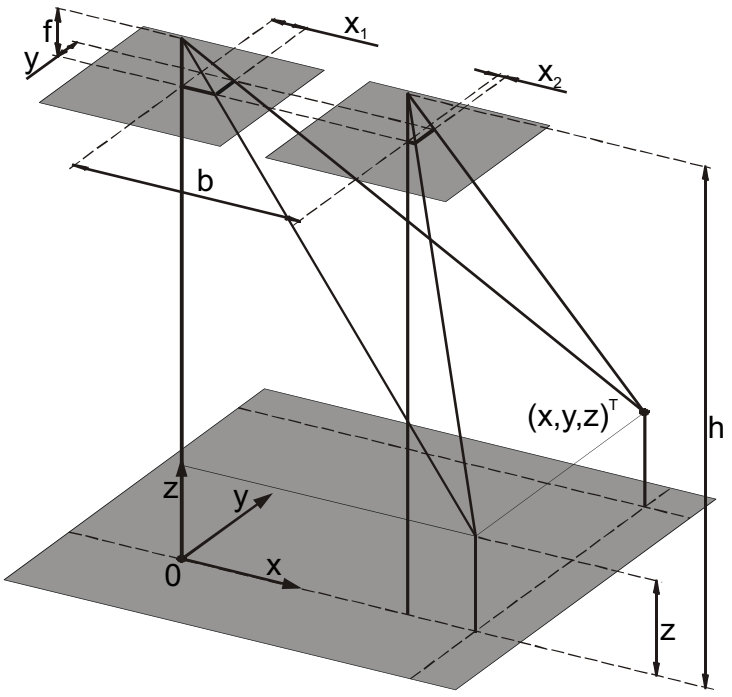

figure 1.1: The principle of stereo-photography.

[3, Grant et al., 1995] describe an apparatus which tackles the problem of correlating the pictures by using a bundle of laser beams to produce a matrix of highlights on a water wave surface. Grant uses one film camera together with a split screen viewing system which permits to photograph the highlights simultaneously from different viewpoints. The experimental arrangement is illustrated in figure 1.2.

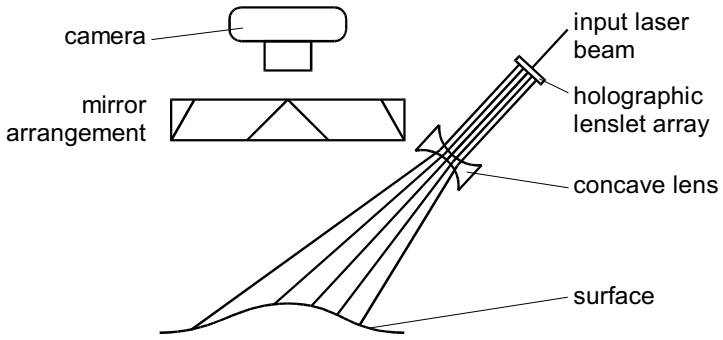

figure 1.2: Split-screen, single-camera, laser-matrix, stereogrammetry instrument for topographical water wave measurements.

Another measurement method is based on the Moiré-effect. [4, Grant et al., 1990] describe a method in which light is projected through a grating onto a water wave surface. The pattern on the water is viewed by a camera through a similar grating. The result is a fringe pattern photograph which can be interpreted as a discrete level-map of the surface. Unfortunately the calibration and tracking of the fringes are complex operations. The water has to be dyed in order to get sufficient contrast.

Further methods use the projection of a regular pattern onto the surface. From the recorded, disturbed pattern the surface of the wave can be calculated.

Other approaches use the effect of light refraction at the water surface. The disadvantage is, that it is usually necessary to mount components like the light source or the camera under water.

For further information about optical measuring methods of water wave surfaces an extensive literature-search is provided on the web pages of the University of Twente by [5, J. H. Westhuis, 1996].

1.3 Objectives of the Present Study

The aim of this study is to develop another measuring method. It is not the claim of this work to develop a completely new measuring principle but to consider a number of factors which meet the demands of offshore engineers above all. Instead of optimising an existing measuring system the procedure of evolving and realising an idea is practised. In the run-up of this study the following boarder conditions have been defined:

- The measurement process must not affect the waves in any way.
- The system should allow continuous measurements to enable the study of wave motions and the process of interaction with offshore structures.
- The system should record and evaluate large scale wave surfaces.
- The process of calibrating and setting up should be simple to enable measurements in rough conditions for example at sea.
- The result should be a mobile, low cost measuring system.

2 Experimental Set-up

2.1 Idea

Optical as well as pressure sensor methods affect waves the least. Optical systems usually can be mounted completely above the water surface. This is of advantage in rough conditions, especially when a mobile measurement system is needed. The device should be able to measure every kind of large scale waves. This includes waves with very small as well as very large wave-slope gradients. Measurements based on light refraction, on Moiré patterns or on the reflected intensity of light are usually dependent on the wave-slope gradient. Therefore these methods normally cover only a certain range of wave shapes. For instance it is difficult to measure large wave-slope gradients with light refraction methods because of the high deflection of the light. The measurement of the water heights along a certain number of sharp focused light beams is independent on these influences. Due to the reflecting quality of a water surface there will be a highlight where a beam meets the water surface. The use of light beams allows to use photographic techniques for recording the measurements. A camera records the data of each measuring point at the same time. This is of benefit, because waves which are interacting with offshore structures, are not stationary relative to the measurement installation.

In laboratory conditions it is favourable to depart from the objectives defined in chapter 1.3 and to mount the light source below the water surface. This is possible when the measurements are done at a basin with a transparent bottom. This arrangement is recommendable because it allows to use less expensive components. For instance, a comparable bright light source is needed to receive highlights on the water surface which are bright enough to be recordable by a camera. By adding some light reflecting material to the water like fine loam the light beams become visible in the water. The light is invisible outside the water. The highlights, due to the reflective quality of water, are replaced in the experiment with the ends of the visible parts of the light beams. The light beams shine brighter and more constant than the highlights would do. The advantage of fitting the light source opposite to the camera (below the the water surface while the camera is mounted

above the water surface) is justified in the light reflection qualities of small particles. The wave length of visible light is between $4 \cdot 10^{-7}$ m and $7 \cdot 10^{-7}$ m. The diameter of fine loam particles, which ranges within the bounds of some 10^{-5} meters, is at least one dimension larger than the wave length of light. In this case, according to Gustav Mie, who published a solution to this problem in 1908, the forward scattered light intensity increases considerably compared to the sideways and backwards scattered light (figure 2.1). According to these reasons it is possible to use a cheaper, fade light source and a camera-lens system of commercial quality.

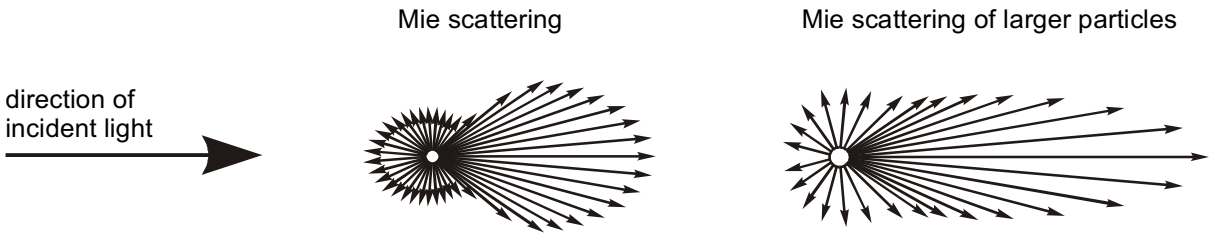

figure 2.1: Mie scattering for homogeneous spherical particles. Long arrows indicate high reflection of light.

The coordinates of the beam end points on the water surface on the picture can be used as a measure for the water height at each measuring point. To calculate the water heights from this information it is necessary to know the camera position, the scale of the picture and the position of the laser beams relative to the camera. Each light beam has a different distance to the camera. Thus each light beam is pictured with a different scale. Therefore the same change of coordinates in the picture indicates an individual change of water height for each measuring point. From there it is necessary to assign the points in the picture to each light beam or measuring point.

Figure 2.2a shows a schematic picture of a horizontal and smooth water surface and nine sharp focused light beams. The numbered end points of the visible part of the beams mark the still water surface or zero levels. Even though figure 2.2a is two dimensional, it can be easily recognised that the laser beams are arranged in a square with beam 1 left hand in the front and beam nine on the right side in the last range. Figure 2.2b shows the end points of the beams from the same position while the surface is wavy. Because of refraction at the water surface the beams themselves appear smeary or disappear completely. Only the end points on the

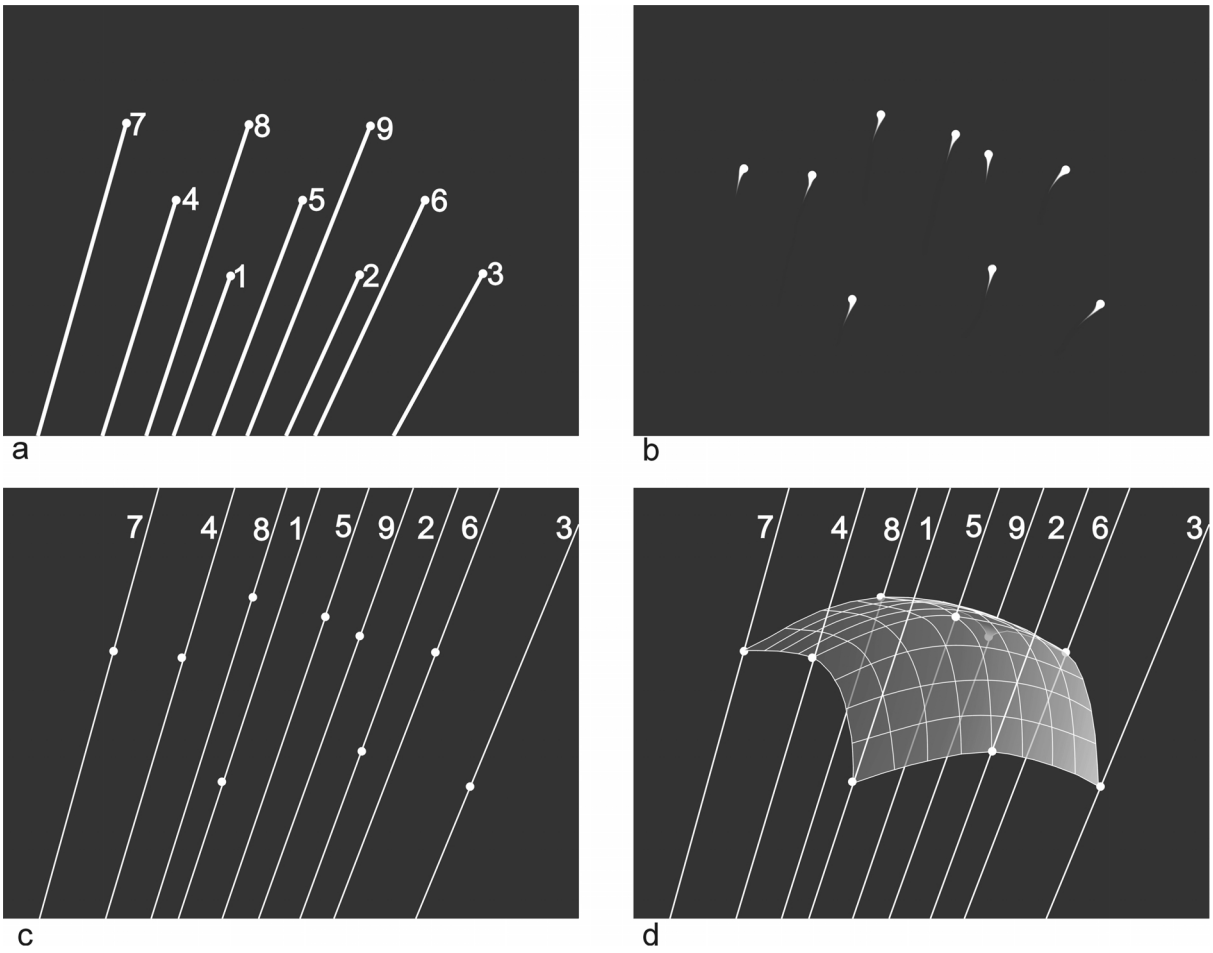

figure 2.2: Schematic pictures of assigning the two dimensional photographic information to the measuring points, scattered in three dimensions.

a) light beams and light points on the still water surface

b) highlights on a wavy water surface

c) into picture projected lines of possible locations of beam end points

d) to the measuring points assigned light points, spanned with a three dimensional surface.

water surface are visible clearly. Because of the bent surface the points are not arranged in a regular pattern anymore like in figure 2.2a. It is impossible to assign the beams reliable to the measuring points.

With the knowledge of the positions of the laser beams relative to the camera as well as the scale of the picture, the laser beams can be easily projected into the photograph. The projected laser beams can be imagined as straight lines in the picture like shown in figure 2.2c. Because of refraction these lines are different from the photographed beams in figure 2.2a, but since there are no refraction effects

effective on and above the water surface, these lines cross the pictured laser beams at their end points on the water surface. Each of these numbered lines represent all possible locations for the end points of a certain laser beam in the picture. On each line there is exactly one light point which can be assigned to the measuring point by the number of the line. Finally the wave surface can be reconstructed and interpolated like indicated in figure 2.2d.

2.2 Components

For the beams, the sharp focused light of a laser is the most useful alternative. In this experiment a 10 mW helium-neon laser manufactured by HUGHES was made available (wavelength: $0.632 \cdot 10^{-6}$ m). As light reflecting particles white wall paint turned out to be a good choice when a fade laser is used. With a sufficient bright laser it would be possible to mount the whole measuring system above the water surface and to do the experiment without dying the water. A fade laser might be kept over the sea level by using lighting wires or pipes equipped with mirrors. The naturally existing plankton is supposed to be suitable to reflect sufficient light.

The laser beam can be split up easily into a diverging bundle of beams by Fraunhofer diffraction at two, 90 degrees crossed gratings. The first grating divides the beam into a row of light beams. The row of beams meets the second grating where every single beam is split up at the same principle, but perpendicular to the first direction. The intensity of the outer beams decreases like illustrated in figure 2.3: Graph (a) shows the main peak of the Fraunhofer diffraction pattern like it would appear if there were only one single slit. Graph (b) describes the light intensity behind a seven slit shield while its maximums are located on graph (a). Graph (c) considers that the light intensity of the laser beam is not constant, but ideal Gauss-shaped. The light intensity I in dependence on the deflection Θ (graph c) can be determined with equation (2.1) [6, Hecht, 1974]:

$$I(\Theta) = \frac{I_0}{N^2}\left(\frac{\sin(\beta)}{\beta}\right)^2 \cdot \left(\frac{\sin(N\cdot\alpha)}{\sin(\alpha)}\right)^2 \cdot e^{-const\cdot\Theta^2} \qquad (2.1)$$

while

$$\alpha = k\cdot a\cdot \sin(\Theta)/2 \qquad (2.2)$$

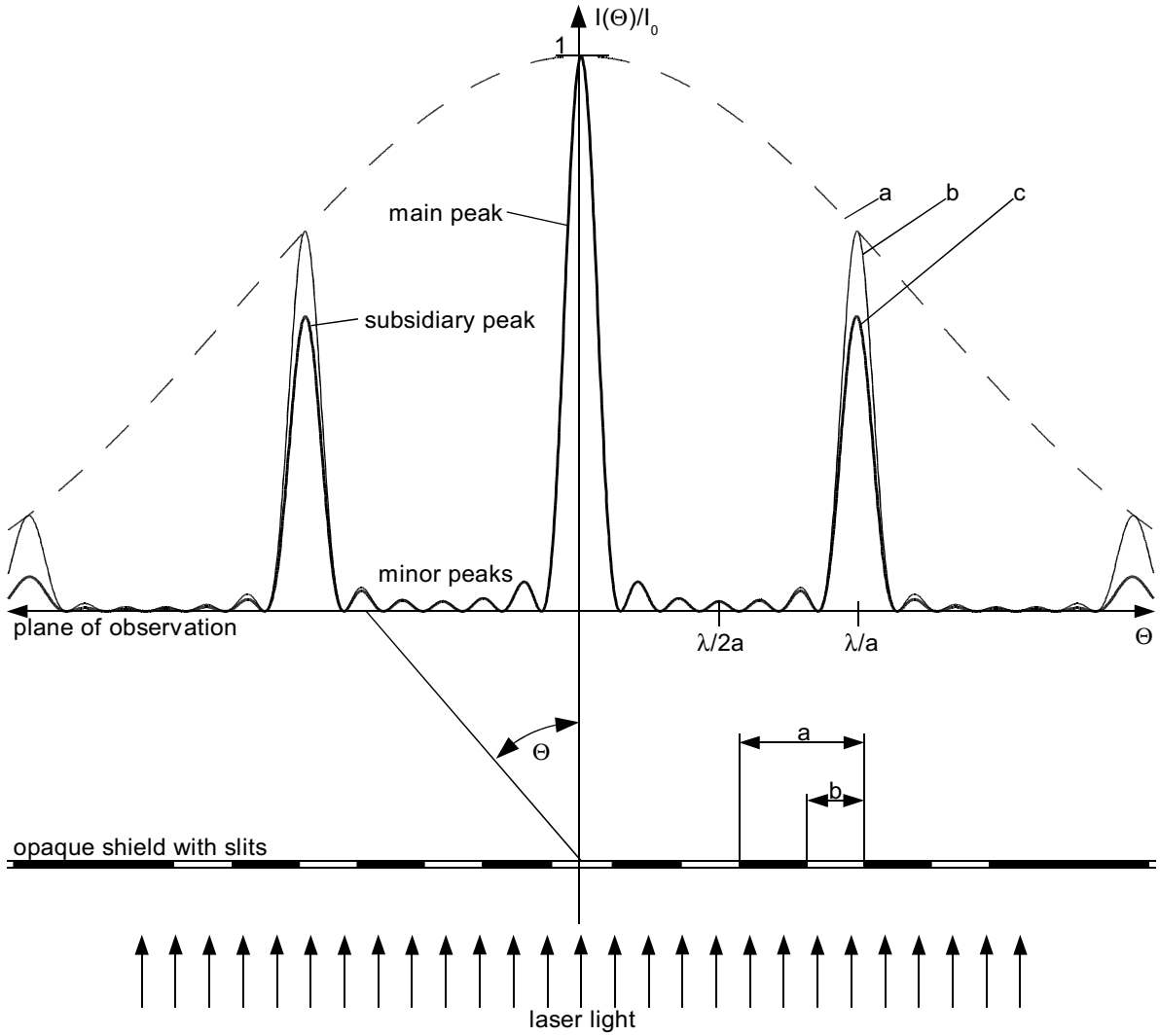

figure 2.3: multiple slit pattern (a=3b, N=7, aperture not true to scale)

I_0 is the intensity of the entering light, N the number of slits and 2α the phase difference between two waves arriving at a point on the plane of observation. β can be determined by

$$\beta = k \cdot b \cdot \sin(\Theta)/2 \tag{2.3}$$

In (2.2) and (2.3) the factor k is the propagation number and dependent on the wave length λ of the entering light:

$$k = \frac{2 \cdot \pi}{\lambda} \tag{2.4}$$

The quantities a and b consider the slit geometry (figure 2.3).

In equation (2.1) the factor I_0/N^2 normalises the graph to the entering laser intensity. The second factor $(\sin(\beta)/\beta)^2$ is responsible for the enveloping shape (graph a in figure 2.3). The third factor $(\sin(N\cdot\alpha)/\sin(\alpha))^2$ is the superimposition of two waves with the same amplitude but differing wavelengths, which leads to the periodical wave train of each one high peak (main and subsidiary peaks) and - depending on N - several minor peaks. With the last factor $e^{-const\cdot\Theta^2}$ the influence of the Gauss-shape of the laser beam can be considered.

Increasing the number of slits N raises the number of minor peaks but decreases their height. The height of the main and subsidiary peaks keeps constant while they become more narrow or sharp. The location of the main and subsidiary peaks remain at the same angle Θ. By increasing the wave lenght λ, as well as by decreasing the distance a of the slits the beams can be fanned out wider. The subsidiary peaks can be enlarged by decreasing b. In this experiment the grating MGP-80 with 80 line pairs per mm by the Newport Corporation is used.

A square diaphragm let pass only the bright beams of the centre which are useful for the measurement, and stops the fade beams of higher order.

A CCD-camera allows to evaluate the pictures immediately without a delay due to the processing of footage and it is useful for automating the evaluation with the help of a computer. It is also possible to record a film for the study of wave motions or the process of interaction with offshore structures. Here the Pulnix TM-6EX, the Nikon lens NIKKOR 50mm 1:1.8 and the frame grabber card WinTV with the chipset

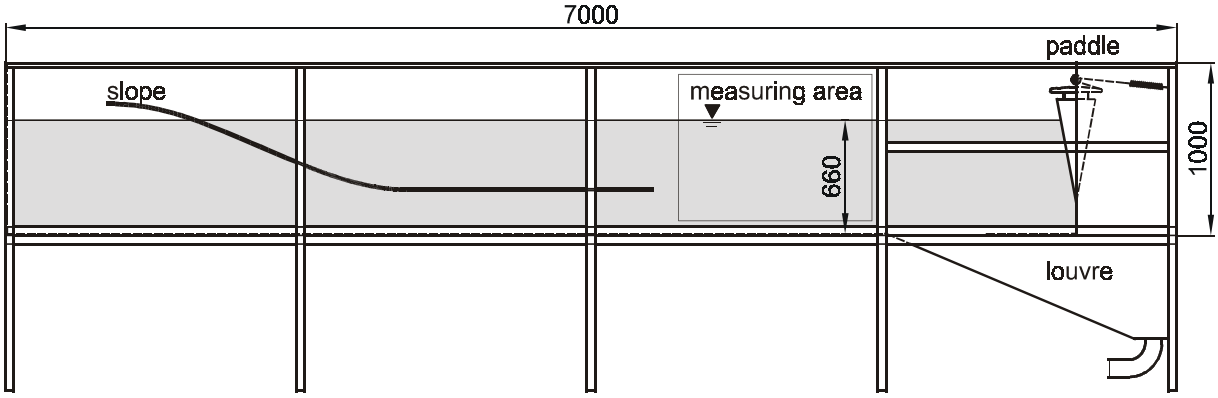

figure 2.4: wave canal

BT848 by Haupauge is used for the data aquisition. The camera has an interlaced resolution of 768 x 575 pixel at 15 pictures per second.

For the creation of water waves as a measuring and test object a transparent wave canal is of great use (figure 2.4). The waves are created by a cyclical forward and backward moving paddle at one end of the canal. The power supply of the paddle drive is controlled by a signal generator which allows to alter the wavelength and amplitude of the waves. By overlaying the signals of two generators, it is possible to create periodical recurrent wave trains. The opposite side of the wave canal is equipped with a slope or beach which keeps the influence of reflected waves to a minimum.

Figure 2.5 gives an overview of the finally realised experimental set-up.

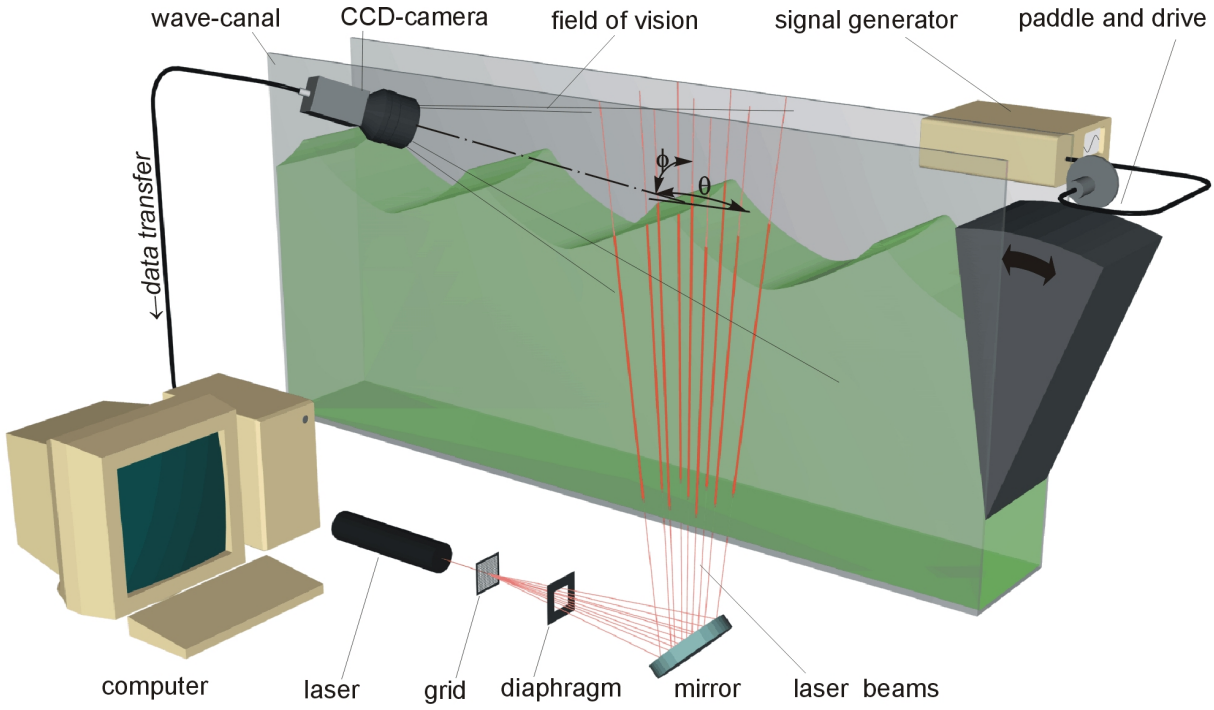

figure 2.5: experimental set-up

3 Evaluation

3.1 Calibration Procedure

3.1.1 Definition of Coordinate Systems

For the measuring of a three dimensional surface with only one camera it is essential to know firstly the position of the camera and secondly the position of the laser beams respectively the measuring points relative to the camera. These positions can be specified in a coordinate-system. On principle any coordinate-system would do, but to make things simple, it is advantageous to define the two following coordinate-systems:

The first system should fulfil two conditions: On the one hand it must be easy to measure the direction and position of the laser beams in this coordinate-system and on the other hand it should be an useful reference for the measured waves like the still water surface or a plain parallel to the still water surface. In this case it is useful

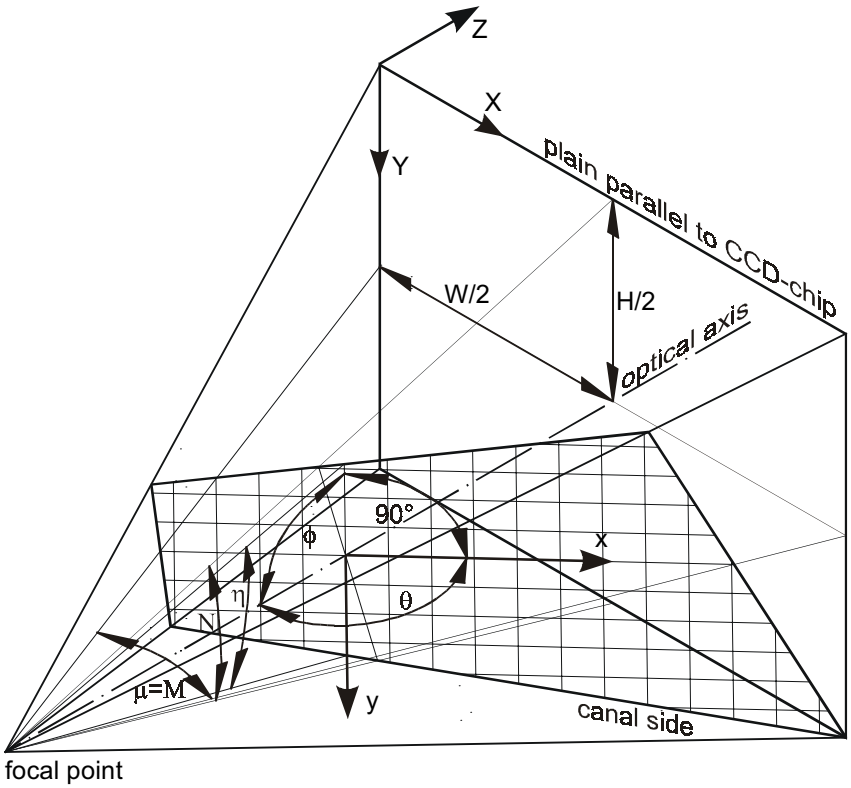

figure 3.1: General idea of the geometry of camera position, angles of view and definition of the coordinate systems.

to define the first system parallel to the wave-canal and to the still water surface. The second system should be parallel to the CCD-chip respectively the measuring picture, because the final measuring picture is written in this coordinates anyway.

The two systems are shown in figure 3.1. The first system (x,y,z - canal system) is parallel to the canal side with its origin in the intersection point of the lenses optical axis z and the canal side. The x-axis is parallel to the still water surface and counts positive to the right from the cameras point of view. The y-axis is perpendicular to the still water surface and points downwards. The second system (X,Y,Z - camera system) comes from the first by turning it around the x-axis and afterwards around the new created Y-axis. This system is moved into the upper left corner of the pixel picture. By defining the coordinate system in this way, the pixels to the right are counted into positive x-direction and downwards into positive y-direction, like most picture processing programs do. The Z-axis is defined perpendicular to the picture plane and positive into the line of vision. The optical axis of the camera lens is parallel to the Z-axis.

3.1.2 Camera Adjustment

The camera is positioned such that the wave surface with all measuring points fits the field of vision. For the calculation of the water height at each measuring point it is necessary to know the camera position relative to the laser beams or to the canal. The orientation of the camera relative to the canal can be described by the two angles ϕ and θ like shown in figure 3.1 (compare also figure 2.5, experimental set-up). To measure these angles directly in the set-up with a protractor is not very handy, time consuming and easily inaccurate. It is more convenient to determine the camera position with the help of a calibration picture.

For that purpose, first of all is to guarantee that the camera orientation comes from the further up explained rotations of the camera coordinate system. This can be guaranteed during the adjustment as follows: Firstly the camera is put roughly perpendicular to the canal side (figure 3.2a). It is easier to do the fine adjustment later. Secondly the camera is turned around the x-axis (canal system) (figure 3.2b). By this turning the Y-achsis of the camera system is created. Afterwards the camera can be turned around this new Y-axis until the measuring area is within the field of vision (figure 3.2c). For the calibration picture a graph paper is fixed on the canal

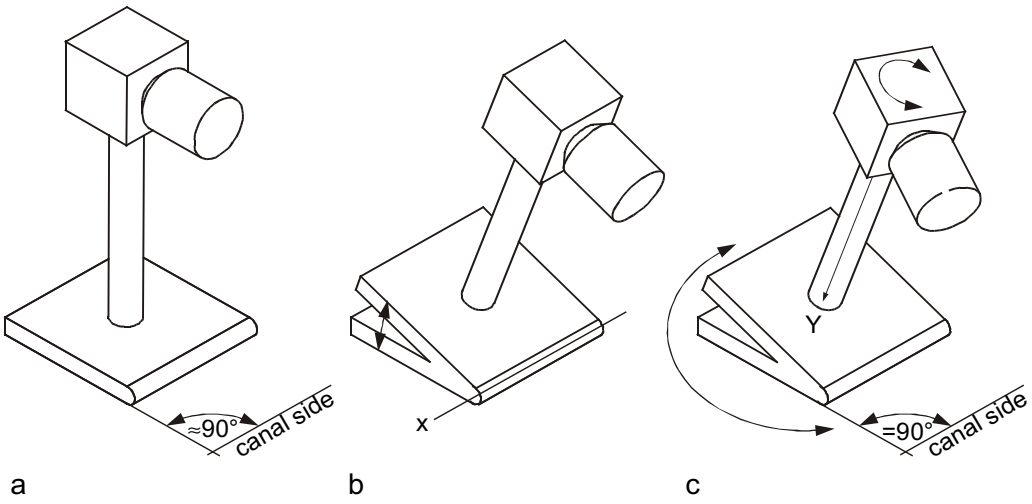

figure 3.2: Set-up of the camera: a) Camera adjusted roughly perpendicular to the canal side. b) Turning camera around x-axis c) Turning camera around new Y-axis until the calibration picture covers the whole field of vision. Then turning of whole stand around the y-axis until the projection of the central, horizontal line of the graph paper is parallel to the picture. The x-axis is parallel to the canal now.

side. The graph paper should cover the whole field of vision and has to be adjusted horizontally by fitting it parallel to the water surface. Finally the fine adjustment is done: The camera is positioned correctly when the horizontal graph paper line which runs through the centre of the frame, is pictured parallel to the boundary of the photo like shown in figure 3.3. This can be achieved by turning the camera inclusive its stand or tripod carefully around the vertical axis (y-achsis) (fig. 3.2c).

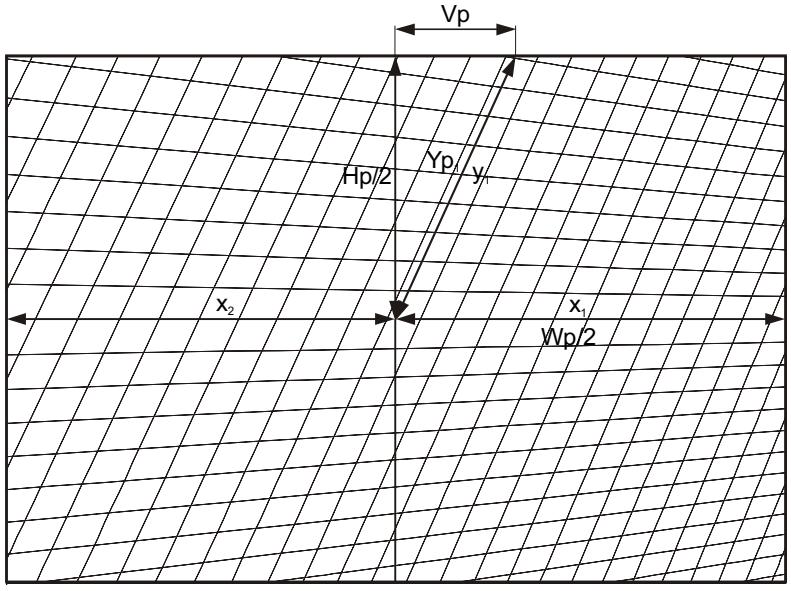

figure 3.3: Projection of the graph paper (thin lines) into the calibration picture.

3.1.3 Calculating the Camera Position

The measures in picture 3.3 are useful for the determination of the angles ϕ and θ. Capital letters and a small p (for pixel) indicate that the measure refers to a length measured in pixel. Small variable names indicate that the measure refers to a length in millimetres, here read from the photographed graph paper.

To calculate the angles ϕ and θ, two imagined triangles in the experimental set-up are of use. In figure 3.4 these triangles are extracted from figure 3.1. The first triangle is determined by z, ν and y_1, the second is determined by z, μ and x_1. y_1 and x_1 can be measured directly in the calibration picture (figure 3.3). μ and ν can be found with the help of the optical opening-angles of the system lens-adapter-camera. For determining these angles, two pictures of a graph paper are taken in different distances (figure 3.5). The paper has to be parallel to the CCD-chip. The distance between the graph paper positions is Δz. The longer Δz, the more exact is the calculation. $M = \mu$ is the horizontal angle of view of the rectangular CCD-chip (figure 3.1). N is the vertical angle of view. w_1 and w_2 are the width of the pictured areas. w_1 and w_2 can be read from the graph paper in the picture. The horizontal

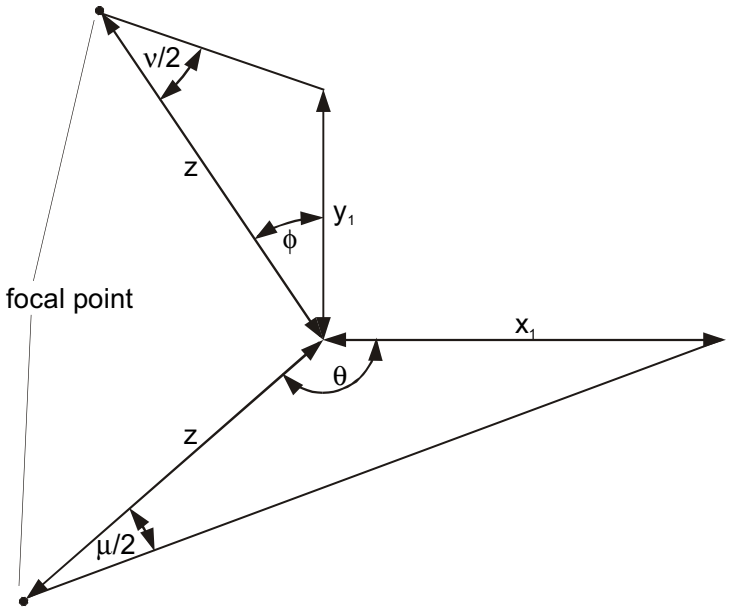

figure 3.4: Two triangles between the focal point of the camera lens and the canal surface. Here the triangles are folded into the two dimensional paper plane.

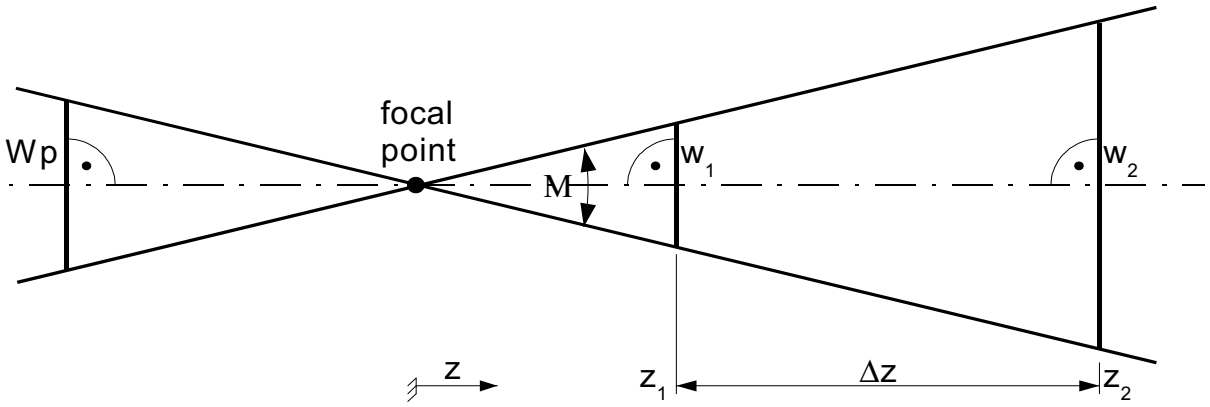

figure 3.5: Determining the angles of view by taking two pictures at z_1 and z_2.

angle of view M can be calculated with:

$$\mu = M = 2 \cdot \arctan\left(\frac{w_2}{2 \cdot z_2}\right) \tag{3.1}$$

The exact position of the focal point is more difficult to determine than the distance Δz between the two graph paper positions. Thus z_2 is calculated with:

$$z_2 = \frac{w_2 \cdot \Delta z}{(w_2 - w_1)} \tag{3.2}$$

Analogous to M, N is:

$$N = 2 \cdot \arctan\left(\frac{h_2}{2 \cdot z_2}\right) \tag{3.3}$$

in which h_2 is the height of the second pictured area in millimetres.

On the canal side the measure x_1 is horizontal and y_1 is vertical. x_1 in the picture is still horizontal but y_1 in the picture is not vertical (compare figure 3.3). Consequently the angle μ = M and ν is a bit larger than N, namely:

$$\nu = 2 \cdot \left(\frac{Yp_1 \cdot 2 \cdot \tan\left(\frac{N}{2}\right)}{Hp}\right) \tag{3.6}$$

Which is developed from the following two equations (compare figure 3.1 and 3.3):

$$\tan\left(\frac{N}{2}\right)=\frac{Hp}{2\cdot z} \quad ; \quad \tan\left(\frac{\nu}{2}\right)=\frac{Yp_1}{z} \qquad \text{(3.4); (3.5)}$$

by eliminating z. Hp is the calibration picture height in pixel and $Yp=\sqrt{Hp/2^2+Vp^2}$ also in pixel (figure 3.3). For determining ϕ and θ with the help of the triangles in figure 3.4 it is necessary to calculate z. This can be done with the help of the triangle shown in figure 3.6. The variables x_1 and x_2 can be measured in the calibration picture (figure 3.3). μ is determined by equation 3.1. From the following two equations (sine theorem) a solution can be developed for determining z by eliminating α.

$$\frac{x_2}{\sin\left(\frac{\mu}{2}\right)}=\frac{z}{\sin(\alpha)} \quad ; \quad \frac{x_1}{\sin\left(\frac{\mu}{2}\right)}=\frac{z}{\sin(\pi-\mu-\alpha)} \qquad \text{(3.7); (3.8)}$$

leading to

$$z=\frac{x_2\cdot x_1\cdot\left(\cos\left(\frac{\mu}{2}\right)\cdot\sin\left(\frac{\mu}{2}-\pi\right)+\sin\left(\frac{\mu}{2}\right)\cdot\cos\left(\frac{\mu}{2}-\pi\right)\right)}{-\sqrt{\left(-2x_1\cdot\sin\left(\frac{\mu}{2}-\pi\right)\cdot x_2\cdot\sin\left(\frac{\mu}{2}\right)+x_1^2+2x_1\cdot\cos\left(\frac{\mu}{2}-\pi\right)\cdot x_2\cdot\cos\left(\frac{\mu}{2}\right)+x_2^2\right)\cdot\sin\left(\frac{\mu}{2}\right)}}$$

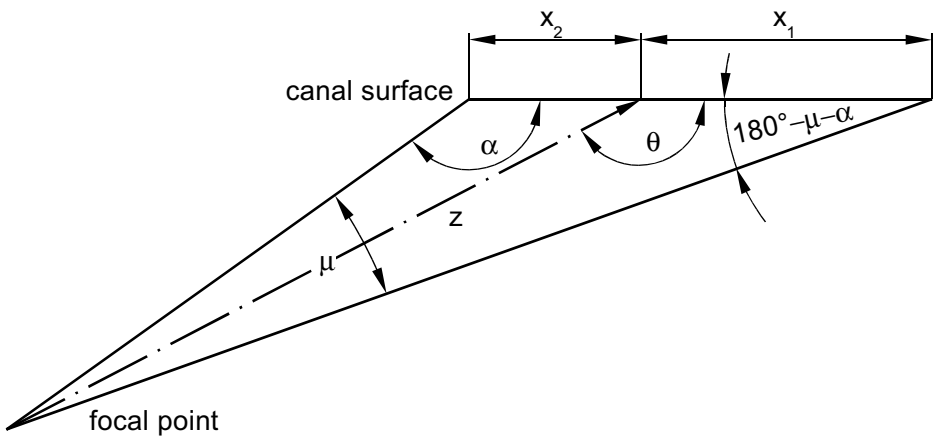

figure 3.6: Distance of intersection point of canal surface and optical axis to focal point.

(3.9)

Finally the equations for determining θ and ϕ can be set up. In figure 3.4 the following equation apply (sine theorem):

$$\frac{z}{\sin\left(180° - \frac{\mu}{2} - \theta\right)} = \frac{x_1}{\sin\left(\frac{\mu}{2}\right)} \tag{3.10}$$

From (3.10) follows:

$$\theta = \pi - \left(\frac{\mu}{2}\right) - \arcsin\left(\frac{z \cdot \sin\left(\frac{\mu}{2}\right)}{x_1}\right) \tag{3.11}$$

Analogous an equation for ϕ can be found, namely:

$$\phi = \pi - \left(\frac{\nu}{2}\right) - \arcsin\left(\frac{z \cdot \sin\left(\frac{\nu}{2}\right)}{y_1}\right) \quad ; \quad \phi = -\left(\frac{\nu}{2}\right) + \arcsin\left(\frac{z \cdot \sin\left(\frac{\nu}{2}\right)}{y_1}\right) \tag{3.12); (3.13}$$

Equation (3.12) applies when the camera is mounted below the water surface (ϕ > 90°) and (3.13) when the camera is mounted above the water surface (ϕ < 90°). The calibration is reasonably precise, when ϕ and θ are sufficiently larger or smaller than 90°. In this study the calculation was practicable for angles between approximately 15° and 80° and 105° and 170° for ϕ and for angles between 10° and 80° and 100° and 170° for θ. Out of this ranges the calculation is not very stable. If the angles are close to 90°, the difference between x_1 and x_2 and the measure Vp become very small. If the angles are close to 0° or 360°, it is not possible to read the graph paper any more.

3.1.4 Transformation Matrixes between the Coordinate Systems

The positions of the laser beams is measured in canal coordinates. The camera provides its picture information in camera coordinates. For calculating the water height in one of these coordinate systems, it is necessary to transform the data between these systems. Before doing the transformations, the turning angles of the

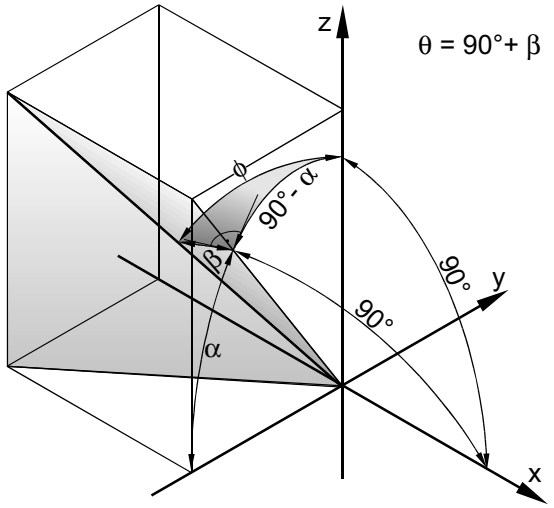

figure 3.7: Calculating the turning angles α and β from ϕ and θ.

coordinate systems have to be calculated from the angles ϕ and θ. α is the turning angle around the x-axis and β is the turning angle around the Y-axis. β is simply calculated by:

$$\beta = \theta - \pi/2 \tag{3.14}$$

For calculating α, the spherical triangle illustrated in figure 3.7 is of use (small, grey triangle, determined by ϕ, β and $90° - \alpha$). For the rectangular, spherical triangle applies:

$$\cos(\phi) = \cos(\pi/2 - \alpha) \cdot \cos(\beta) \tag{3.15}$$

Equation (3.14) and (3.15) are leading to:

$$\alpha = \frac{\pi}{2} - \arccos\left(\frac{\cos(\phi)}{\cos\left(\theta - \frac{\pi}{2}\right)}\right) \tag{3.16}$$

Now the transformation with the matrixes can be done. The first two matrixes describe the transformation from the canal system into the camera system. For the first matrix (turning around the x-axis) the transformation of the y-coordinate is explained in figure 3.8. The other transformations work similar. The transformations are done without moving the origin of the coordinate system. A movement of the coordinate system from the canal side to the focal point of the camera is not

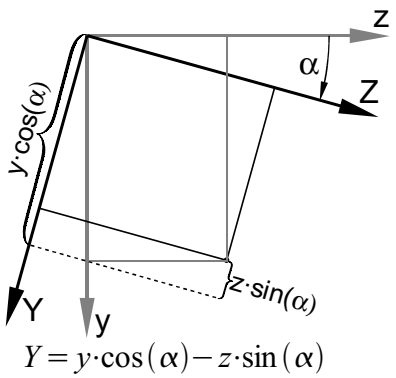

figure 3.8: Example: Transforming the y-coordinate of a point into a rotated coordinate system.

necessary. It would only concern the Z-coordinates. Since the CCD-chip is parallel to the X - Y - plane, the Z-coordinates of the picture data are always zero. The turning around the x-axis is described by:

$$\begin{bmatrix} x' \\ Y \\ z' \end{bmatrix} = \begin{bmatrix} 1 & 0 & 0 \\ 0 & \cos(\alpha) & -\sin(\alpha) \\ 0 & \sin(\alpha) & \cos(\alpha) \end{bmatrix} \cdot \begin{bmatrix} x \\ y \\ z \end{bmatrix} \tag{3.17}$$

The turning around the Y-axis is described by:

$$\begin{bmatrix} X \\ Y \\ Z \end{bmatrix} = \begin{bmatrix} \cos(\beta) & 0 & -\sin(\beta) \\ 0 & 1 & 0 \\ \sin(\beta) & 0 & \cos(\beta) \end{bmatrix} \cdot \begin{bmatrix} x' \\ Y \\ z' \end{bmatrix} \tag{3.18}$$

For the transformation matrix follows:

$$\begin{bmatrix} X \\ Y \\ Z \end{bmatrix} = \begin{bmatrix} \cos(\beta) & -\sin(\beta)\cdot\sin(\alpha) & -\sin(\beta)\cdot\cos(\alpha) \\ 0 & \cos(\alpha) & -\sin(\alpha) \\ \sin(\beta) & \cos(\beta)\cdot\sin(\alpha) & \cos(\beta)\cdot\cos(\alpha) \end{bmatrix} \cdot \begin{bmatrix} x \\ y \\ z \end{bmatrix} \tag{3.19}$$

The matrix for transformations from the camera coordinate system into the canal system can be obtained by mirroring the matrix in (3.19) at its main diagonal:

$$\begin{bmatrix} x \\ y \\ z \end{bmatrix} = \begin{bmatrix} \cos(\beta) & 0 & \sin(\beta) \\ -\sin(\beta)\cdot\sin(\alpha) & \cos(\alpha) & \cos(\beta)\cdot\sin(\alpha) \\ -\sin(\beta)\cdot\cos(\alpha) & -\sin(\alpha) & \cos(\beta)\cdot\cos(\alpha) \end{bmatrix} \cdot \begin{bmatrix} X \\ Y \\ Z \end{bmatrix} \tag{3.20}$$

3.2 Calculation of the Wave Shape

3.2.1 Convention of Symbols

The necessary equations for calculating the water heights at each measuring point can be found in figure 3.9. To distinguish between vectors in camera coordinates and vectors in canal coordinates, all vectors in camera coordinates have a doubled letter as a variable name. For example the vector showing from the focal point of the camera lens along the Z-axis to the canal side is named $\vec{O}$ in canal

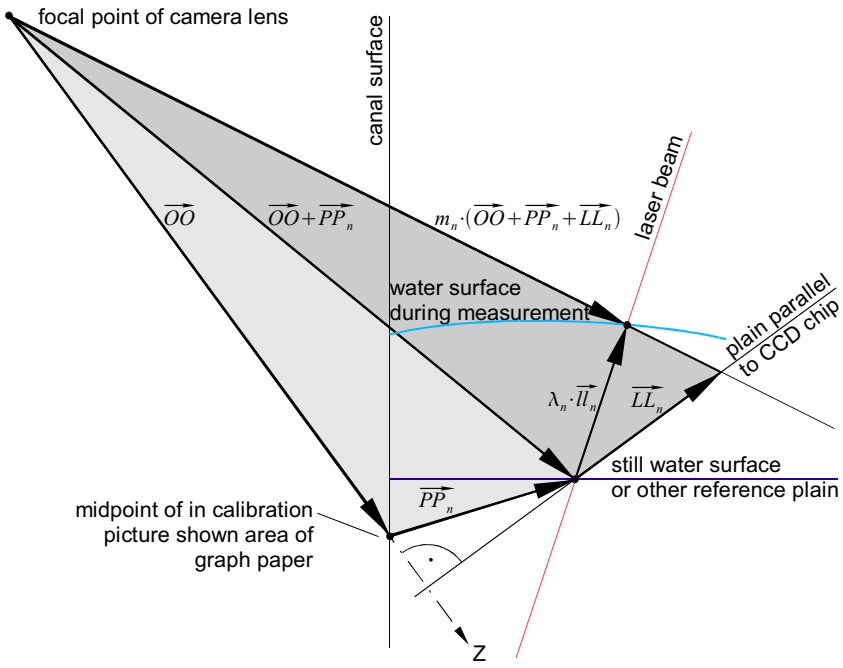

figure 3.9: Relations for calculating the water height at each measuring point.

coordinates and $\overrightarrow{OO}$ in camera coordinates. Vector components are marked with the indexes $_X$, $_Y$, $_Z$ if they are given in camera coordinates and with $_x$, $_y$, $_z$ if they are given in canal coordinates. The index $_n$ means that this component is existing n-times while n is the number of measuring points. In this experiment n is nine. In figure 3.9 all vectors are displayed in camera coordinates. This is advantageous because the x- and y-components of $\overrightarrow{OO}$ are both zero in contrast to $\vec{O}$ which three components are all different from zero.

3.2.2 Calculation

The vector $\overrightarrow{ll}_n$ represents the water height at each measuring point measured from the reference plain. The central task is to calculate this vector. The direction of $\overrightarrow{ll}_n$ can be described by the diverging-angle of the laser beam bundle. This angle can be determined for example by measuring the distance between the beams at two plains with a certain space. The length λ of $\overrightarrow{ll}_n$ is unknown. From equation (3.21) λ can be derived (figure 3.9):

$$\overrightarrow{OO}+\overrightarrow{PP}_n+\lambda\cdot\overrightarrow{ll}_n-m\cdot(\overrightarrow{OO}+\overrightarrow{PP}_n+\overrightarrow{LL}_n)=0 \qquad (3.21)$$

The vector $\overrightarrow{OO}$ is known: Its X and Y components are zero and the Z component equals z of equation (3.9). $\overrightarrow{PP_n}$ are n Vectors which describe the location of n intersection points of each laser beam with the still water surface or reference plane. There are two ways of determining these coordinates. One way is calculating the coordintes with equations (2.1) to (2.4). It is necessary to know the distance between the optical grating and the reference plain. Additional the position of the laser beams relative to the canal have to be known for calculating the Vectors $\overrightarrow{PP_n}$. The other way is to measure the positions of the laser beams directly on the still water surface. In this study the measurement is done by marking the positions of the laser beams on a graph paper lying on the water. The paper fits tightly at the canal side. All measures rectangular to the canal side plus the glass thickness give the z-coordinates of the light points. The measures parallel to the canal side provide the x-coordinates. x = 0 is the graph paper line that starts vertical above the point O. The y-coordinate equals the water height above O and is identical for every light point. The vector position is received in canal coordinates. After transforming this vector into camera coordinates, a small error arises due to refraction at the canal wall. This error can be considered by Snellius law which is in the case of vertical refraction:

$$n_1 \cdot \sin(\gamma_{1,n}) = n_2 \cdot \sin(\delta_{1,n}) \tag{3.22}$$

n are the refraction numbers. n_1 is 1 for air and n_2 is 1.46 for glass. $\delta_{1,n}$ are the angles of refraction in vertical direction (figure 3.10). $\gamma_{1,n}$ are the vertical angles of view from the camera to each measuring point. The vertical and horizontal angles of view γ_n are:

$$\gamma_{1,n} = \arctan\left(\frac{\overrightarrow{(O_n + P_n)_y}}{\overrightarrow{(O_n + P_n)_z}}\right) \quad ; \quad \gamma_{1,n} = \arctan\left(\frac{\overrightarrow{(O_n + P_n)_x}}{\overrightarrow{(O_n + P_n)_z}}\right) \tag{3.23); (3.24}$$

From (3.23) follows for the vertical and the horizontal angle of refraction δ_1 and δ_2:

$$\delta_{1,n} = \arcsin\left(\frac{\sin(\gamma_{1,n})}{1.46}\right) \quad ; \quad \delta_{2,n} = \arcsin\left(\frac{\sin(\gamma_{2,n})}{1.46}\right) \tag{3.25); (3.26}$$

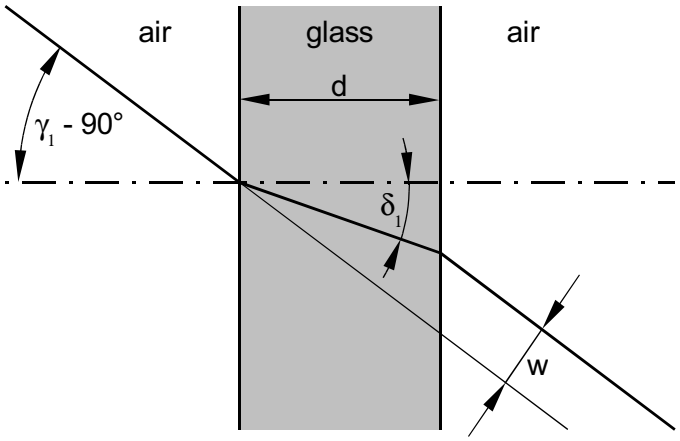

figure 3.10: Refraction at the canal side.

In figure 3.10 for the vertical and the horizontal shifts can be found:

$$w_n = \sin(\gamma_{1,n} - \delta_{1,n}) \cdot \frac{d}{\cos(\delta_{1,n})} \quad ; \quad v_n = \sin(\gamma_{1,n} - \delta_{2,n}) \cdot \frac{d}{\cos(\delta_{2,n})} \qquad (3.27); (3.28)$$

By subtracting v from the x-components and w from the y-components of $\overrightarrow{PP_n}$ the refraction can be considered.

$\overrightarrow{LL_n}$ is the projection of $\overrightarrow{ll_n}$ into the picture plane. Its Z-coordinate is zero while the X- and Y-directions can be measured in the picture. Also the length Λ of $\overrightarrow{LL_n}$ can be measured in the picture. For this purpose the positions of the laser beam endpoints on the reference plain in the pixel-picture are calculated and subtracted from the coordinates of the pictured laser beam end points on the wavy surface. The calculation of the laser beam endpoints in the pixel-picture is just a transformation of the vectors $\vec{O} + \overrightarrow{P_n}$ into camera coordinates and setting its z-coordinate to zero. It is necessary to transform this measure from pixel into mm. This can be done by a magnitude function. To get this function the information of the set-up in figure 3.5 may be used. It follows:

$$MP(Z)_n = \frac{w_2 - w_1}{Wp \cdot \Delta z} \cdot Z_n \qquad (3.29)$$

$MP(Z)_n$ is the magnitude at each light point depending on its distance to the camera Z. Wp is the width of the picture in pixel.

The amount of $\overrightarrow{LL_n}$ equals the product of magnitude and length Λ of $\overrightarrow{LL_n}$ in the pixel picture:

$$LL_{X,n}^2 + LL_{Y,n}^2 = (\Lambda \cdot MP(Z)_n)^2 \tag{3.30}$$

The vectors $\overrightarrow{OO} + \overrightarrow{PP_n}$, $\overrightarrow{ll_n}$ and its projection $\overrightarrow{LL_n}$ are lying in one plain, thus equation 3.31 applies:

$$\overrightarrow{LL_n} \cdot ((\overrightarrow{OO} + \overrightarrow{PP_n}) \times \overrightarrow{lln}) = 0 \tag{3.31}$$

(3.30) has the following solution for $LL_{X,n}$:

$$LL_{X,n} = \pm\sqrt{LL_{Y,n}^2 + \Lambda^2 \cdot MP(Z)_n^2} \tag{3.32}$$

$LL_{X,n}$ in equation (3.31) can be substituted by the right part of (3.32). Solved to $LL_{Y,n}$ follows:

$$LL_{Y,n} = \frac{-\Lambda_n \cdot MP(Z)_n \cdot (PP_{Y,n} \cdot ll_{Z,n} - ll_{Y,n} \cdot OO_Z - ll_{Y,n} \cdot PP_{Z,n})}{\sqrt{(PP_{Y,n} \cdot ll_{Z,n} - ll_{Y,n} \cdot OO_Z - ll_{Y,n} \cdot PP_{Z,n})^2 + (ll_{X,n} \cdot OO_Z + ll_{X,n} \cdot PP_{Z,n} - PP_{X,n} \cdot ll_{Z,n})^2}} \tag{3.33}$$

All vectors of equation (3.21) are known at this point. The two factors λ and m are unknown. Calculating the vector-equation (3.21) leads to a linear system of three equations. This system describes a plain triangle. That means that the triangle can also be defined by two dimensional vectors by turning the coordinate system. Thus one of the equations is dependent on the other two. A solution for m is not needed. One of three equivalent solutions for λ_n is:

$$\lambda_n = \frac{(L_{z,n} \cdot O_y + L_{z,n} \cdot P_{y,n} - O_z \cdot L_{y,n} - P_{z,n} \cdot L_{y,n})}{(l_{z,n} \cdot O_y + l_{z,n} \cdot P_{y,n} + l_{z,n} \cdot L_{y,n} - l_{y,n} \cdot O_z - l_{y,n} \cdot P_{z,n} - l_{y,n} \cdot L_{z,n})} \tag{3.34}$$

In equation (3.34) all quantities are transformed from camera coordinates to canal coordinates. It is more clear for the observer if the water height is declared in canal coordinates.

Finally the vectors describing the wave shape can be calculated by:

$$\overrightarrow{H_n} = \overrightarrow{P_n} + \lambda_n \cdot \overrightarrow{l_n} \tag{3.35}$$

For displaying the measurement in a diagram, $H_{x,n}$ and $H_{z,n}$ have to be used for the x- and z-coordinates of the measuring points, while $H_{y,n}$ represents the water height above this points of the x-z-plane. Depending on the wave shape and the

diverging angle of the laser bundle, the coordinates of the measuring points move slightly. They are fixed for a diverging angle of zero. An example calculation is added in the appendix in the form of a Mathcad 7.0® Worksheet plot . The functioning worksheet (wave evaluation.mcd) is also added on CD-ROM as well as the recorded film (wave.avi), the picture processed film (wavelin.avi) and the result (waveeval.avi). Comments how to use the worksheet are written at suitable positions.

3.2.3 Error Estimation

An error calculation was renounced because the error was easy to estimate: Firstly a picture was taken of the still water surface. Then the water level was risen or lowered and a second picture was taken. From the two pictures it is possible to calculate the difference between both water levels. The calculation can be checked by measuring the distance between both levels directly at the transparent canal wall with a ruler. It's also possible to check if the water height is equal at every measuring point which leads to the conclusion that the calibration of the system was correct. An additional estimation was made by producing waves of the same amplitude. The wave shape was recorded and calculated. The maximal height of the waves was easily to measure at the canal side for a comparison with the calculation.

The difference between the calculated water heights at each measuring point at a still water surface was smaller than 1 mm. The error of the calculated difference of still water levels and the measured difference of still water levels was smaller than 2 mm. This error is independent on the amount of the change of the water level.

The error of the maximal wave height was smaller than 4 mm. The larger deviation appears because of slightly blurred pictures due to the interlacing[1] of the CCD-camera. This error is also independent on the absolute water height. In this study waves from about 30 to 150 mm maximal height were measured. Consequently the error of the measurements is estimated between 14 % for small waves and 3 % for larger waves relative to the maximal height of the wave. For waves larger than 400 mm the error is supposed to be smaller than 1 % relative to the maximal height of the wave.

1 The CCD-chip is read out in two steps: Firstly only every second sensor line is read out and after a short time interval the rest of the sensors. The final picture consists of two interlaced pictures which were taken at different times. If quick motions are recorded, the final picture appears slightly blurred.

4 Outlook

There are a number of suggestions for improving the measuring method which could not been realised in the limited time.

- An automated procedure for reading the coordinates of the highlights from the pictures would save time during the evaluation. This automation could be realised with a computer program which detects gradients of grey values along the lines of calculated possible positions of high lights. The coordinates of the highlights are lying between the two highest gradients of grey values on each line.
- The use of a brighter laser would allow to mount the whole measuring system above the water surface.
- The use of a holographic lenslet array like it is used in [3, Grant et al, 1995] would enable the measurement at more measuring points. The light intensity is more constant over the pattern, while the light intensity decreases significantly at the boarder of the pattern produced with an optical grating in this study.
- The usefulness of the method for the measurement of larger water waves could be tested at a 9.0 x 9.0 x 0.9 m wave basin existing at the Heriot-Watt University.
- The use of optical filters which let pass only light of the wave length of the used laser light source, would enable measurements at daylight.
- The effect of blurred wave pictures can be minimised by using a none interlacing camera or by deleting every second line in the final picture and replacing them with pixels which grey-values have been interpolated between the remaining lines.

5 Bibliography

1. L. H. Holthuijsen; Stereo-photography of ocean waves; *Applied ocean research, Vol. 5, p. 204-210, 1993*
2. O. H. Shemdin; Measurement of short surface waves with stereophotography; *Oceans, p. 568-572, September 1990*
3. I. Grant, Y. Zhao, G. H. Smith and J. N. Stewart; Split Screen, single-camera, laser-matrix, stereogrammetry instrument for topographical water wave measurements; *Applied Optics, Vol. 34, p. 3806-3809, 1995*
4. I. Grant, N. Steward, I. A. Padilla-Perez; Topographical measurements of water waves using the projection moire method; *Applied Optics, Vol. 29, p. 3981-3983, 1990*
5. J. H. Westhuis; Extensive Interactive Report on Literature Search on Water Wave Measurement; *MARIN (Maritime Research Institute Netherlands) and the Department of Applied Mathematics of the University of Twente 1996; retrievable at: http://www.math.utwente.nl/~westhuis/lit/lithome.htm*
6. Eugene Hecht, Alfred Zajac; Adelphi University; Optics; *Addison-Wesley Publishing Company Reading; Massachusetts 1974*
7. Allen Nussbaum; University of Minnesota; Geometric Optics - An Introduction; *Addison-Wesley Publishing Company Reading; Massachusetts 1968*
8. Paul A. Tipler; Physics for Scientists and Engineers; *Worth Publishers Inc. New York 1991*

Appendix

A. Calibration

Calculating the Camera Position

Specification of the system variables:

Measures of magnitude pictures (figure 3.6):

$w1 := 122.8\,mm$
$w2 := 224.2\,mm$
$h1 := 92.5\,mm$
$h2 := 169.8\,mm$
$\Delta z := 835\,mm$

CCD-chip:

$Hp := 576$
$Wp := 768$

Measures of calibration picture (figure 3.3):

$$Y1 := \sqrt{\left(\frac{Hp}{2}\right)^2 + 96^2}$$

$x1 := 104.3\,mm$
$x2 := 97.7\,mm$
$y1 := 78.6\,mm$

The angles of view can be calculated (equations 3.1 - 3.6):

$$z2 := \frac{w2 \cdot \Delta z}{(w2 - w1)}$$

$$N := 2 \cdot \operatorname{atan}\left(\frac{h2}{2 \cdot z2}\right)$$

$$\nu := 2 \cdot \operatorname{atan}\left(\frac{Y1 \cdot 2 \cdot \tan\left(\frac{N}{2}\right)}{Hp}\right)$$

$$\mu := 2 \cdot \operatorname{atan}\left(\frac{w2}{2 \cdot z2}\right)$$

The distance of the intersection point of the canal surface and the optical axis to the focal point is (equations 3.7 -3.9):

$$z := \frac{x2 \cdot x1 \cdot \left(\cos\left(\frac{\mu}{2}\right) \cdot \sin\left(\frac{\mu}{2} - \pi\right) + \sin\left(\frac{\mu}{2}\right) \cdot \cos\left(\frac{\mu}{2} - \pi\right)\right)}{-\sqrt{(-2 \cdot x1) \cdot \sin\left(\frac{\mu}{2} - \pi\right) \cdot x2 \cdot \sin\left(\frac{\mu}{2}\right) + x1^2 + 2 \cdot x1 \cdot \cos\left(\frac{\mu}{2} - \pi\right) \cdot x2 \cdot \cos\left(\frac{\mu}{2}\right) + x2^2} \cdot \sin\left(\frac{\mu}{2}\right)}$$

The position of the camera is defined by the two angles θ and ϕ. The following equations are valid for camera positions above the water surface (equations 3.10 -3.13):

$$\theta := \pi - \frac{\mu}{2} - \operatorname{asin}\left(\frac{z \cdot \sin\left(\frac{\mu}{2}\right)}{x1}\right) \qquad \phi := \frac{-\nu}{2} + \operatorname{asin}\left(\frac{z \cdot \sin\left(\frac{\nu}{2}\right)}{y1}\right)$$

Coordinate Transformation between Canal System and Camera System:

Turning angles of the camera coordinate system
relative to the canal coordinate system (equations 3.14 - 3.16):

$$\alpha := \frac{\pi}{2} - \operatorname{acos}\left(\frac{\cos(\phi)}{\cos\left(\theta - \frac{\pi}{2}\right)}\right) \qquad \beta := \theta - \frac{\pi}{2}$$

Transformation from canal coordinates into camera coordinates (equation 3.17 -3.19):

$$T := \begin{bmatrix} \cos(\beta) & -\sin(\alpha)\cdot\sin(\beta) & -\cos(\alpha)\cdot\sin(\beta) \\ 0 & \cos(\alpha) & -\sin(\alpha) \\ \sin(\beta) & \sin(\alpha)\cdot\cos(\beta) & \cos(\alpha)\cdot\cos(\beta) \end{bmatrix}$$

O in camera coordinates:

$$OO := z \begin{bmatrix} 0 \\ 0 \\ -1 \end{bmatrix}$$

Transformation from camera coordinates into canal coordinates (equation 3.20):

$$t := \begin{bmatrix} \cos(\beta) & 0 & \sin(\beta) \\ -\sin(\alpha)\cdot\sin(\beta) & \cos(\alpha) & \sin(\alpha)\cdot\cos(\beta) \\ -\cos(\alpha)\cdot\sin(\beta) & -\sin(\alpha) & \cos(\alpha)\cdot\cos(\beta) \end{bmatrix}$$

O in canal coordinates:

$$O := t \cdot OO$$

B Calculation of Water Heights

The position and the diverging angles of the laser beams are specified:

Coordinates of measuring points on still water surface:

$y := 120$

$$P := \begin{bmatrix} 41 & 89 & 137 & 41 & 89 & 137 & 41 & 89 & 137 \\ y & y & y & y & y & y & y & y & y \\ 95 & 95 & 95 & 144 & 144 & 144 & 193 & 193 & 193 \end{bmatrix} \text{mm}$$

Direction of laser beams from Pn:

$$l := \begin{bmatrix} -21 & 0 & 21 & -21 & 0 & 21 & -21 & 0 & 21 \\ -549 & -549 & -549 & -549 & -549 & -549 & -549 & -549 & -549 \\ -21 & -21 & -21 & 0 & 0 & 0 & 21 & 21 & 21 \end{bmatrix} \text{mm}$$

The possible positions of the laser beams in the picture are calculated:

Transformation of laser beam end points into camera coordinates:

$PP := T \cdot P$

The next part considers the refraction of the canal glass:

Vektor in canal coordinates from focal point to light point on the still water surface:

$i := 0 .. 8$

$j := 0 .. 2$

$OP^{\langle i \rangle} := -O + P^{\langle i \rangle}$

Angles of refraction (equations 3.23 - 3.26):

$$\delta 1_i := \operatorname{asin}\left[\frac{\sin\left(\operatorname{atan}\left(\frac{OP_{1,i}}{OP_{2,i}}\right)\right)}{1.46}\right] \qquad \delta 2_i := \operatorname{asin}\left[\frac{\sin\left(\operatorname{atan}\left(\frac{OP_{0,i}}{OP_{2,i}}\right)\right)}{1.46}\right]$$

Shift of picture due to refraction (3.27-3.28):

$$w_i := \sin\left(\operatorname{atan}\left(\frac{OP_{1,i}}{OP_{2,i}}\right) - \delta 1_i\right) \cdot \frac{10\ \text{mm}}{\cos\left(\delta 1_i\right)} \qquad v_i := \sin\left(\operatorname{atan}\left(\frac{OP_{0,i}}{OP_{2,i}}\right) - \delta 2_i\right) \cdot \frac{10\ \text{mm}}{\cos\left(\delta 2_i\right)}$$

Applying the shift due to refraction at the canal glass:

$$PP^{\langle i \rangle} := PP^{\langle i \rangle} - \begin{bmatrix} v_i \\ w_i \\ 0 \end{bmatrix}$$

Scale in Pn and projection of measuring points on reference plain into picture plane (equation 3.29):

$$MP_i := \frac{w2 - w1}{Wp \cdot \Delta z} \cdot \left(-OO + PP^{\langle i \rangle} \right)_2$$

$$PPxl^{\langle i \rangle} := \frac{PP^{\langle i \rangle}}{MP_i}$$

PPxl are the positions of the laser end points in camera coordinates measured from the picture mid-point.

Move of coordinate system from picture mid point into upper left corner:

$$PPexpected^{\langle i \rangle} := PPxl^{\langle i \rangle} + \begin{bmatrix} \frac{Wp}{2} \\ \frac{Hp}{2} \\ -PPxl_{2,i} \end{bmatrix}$$

Coordinates of laser beams in the wave pictures. The following matrix contains lines for a film of ten pictures. In the first line are the x-coordinates, in the second line are the y-coordinates and so on.

$$pointcoord := \begin{bmatrix} 299 & 459 & 618 & 222 & 381 & 543 & 148 & 307 & 468 \\ 402 & 413 & 409 & 298 & 308 & 301 & 203 & 208 & 198 \\ 293 & 474 & 643 & 218 & 381 & 555 & 146 & 310 & 472 \\ 416 & 383 & 380 & 310 & 305 & 272 & 207 & 200 & 185 \\ 293 & 468 & 646 & 219 & 394 & 568 & 146 & 317 & 487 \\ 414 & 382 & 352 & 305 & 277 & 231 & 202 & 179 & 147 \\ 306 & 485 & 672 & 224 & 405 & 583 & 152 & 326 & 505 \\ 379 & 342 & 297 & 291 & 240 & 202 & 186 & 149 & 100 \\ 306 & 503 & 674 & 233 & 418 & 585 & 158 & 343 & 506 \\ 367 & 299 & 297 & 261 & 200 & 200 & 159 & 91 & 98 \\ 320 & 507 & 665 & 251 & 427 & 577 & 173 & 349 & 503 \\ 327 & 295 & 318 & 196 & 182 & 224 & 102 & 83 & 134 \\ 338 & 503 & 651 & 256 & 420 & 562 & 183 & 344 & 484 \\ 285 & 307 & 352 & 180 & 220 & 261 & 80 & 104 & 174 \\ 328 & 484 & 634 & 254 & 407 & 551 & 179 & 330 & 471 \\ 288 & 338 & 391 & 193 & 239 & 290 & 99 & 151 & 196 \\ 314 & 472 & 620 & 241 & 396 & 543 & 168 & 317 & 467 \\ 331 & 379 & 415 & 223 & 272 & 304 & 147 & 183 & 204 \end{bmatrix}$$

The number of the index behind "pointcoord" chooses the line of the matrix above for the evaluation:

$\Lambda 2_{0,i} := \text{pointcoord}_{12,i}$

$\Lambda 2_{1,i} := \text{pointcoord}_{13,i}$

This is the part of the matrix pointcoord (representing one single picture) that is evaluated presently:

$$\Lambda 2 = \begin{bmatrix} 338 & 503 & 651 & 256 & 420 & 562 & 183 & 344 & 484 \\ 285 & 307 & 352 & 180 & 220 & 261 & 80 & 104 & 174 \end{bmatrix}$$

This line allows to read a pixel picture of the still water surface to compare it with the calculated results:

$M := \text{BMPLESEN}(\text{"c:\stillw.bmp"})$

Running variables of the read pixel picture:

$o := 0 .. 575$

$p := 0 .. 767$

The following line defines the function "runden" which is necessary for drawing the lines of the possible locations of endpoints into the wave pictures:

$\text{runden}(x) := \text{wenn}(x - \text{floor}(x) < 0.5, \text{floor}(x), \text{ceil}(x))$

This line rounds the coordinates of the laser beam end points to assign the coordinates to the whole number of pixel coordinates in the picture:

$\text{PPexpected}_{j,i} := \text{runden}\left(\text{PPexpected}_{j,i}\right)$

The following line draws the calculated endpoints in a picture from the still water surface to give the possibility to compare the calculated results with a photograph of the still water surface:

$N_{o,p}\left[\text{wenn}\left[\left(o = \text{PPexpected}_{1,0}\right)\cdot\left(p = \text{PPexpected}_{0,0}\right) + \left(o = \text{PPexpected}_{1,1}\right)\cdot\left(p = \text{PPexpected}_{0,1}\right) + ...\right], o\right]$

Normalizing of l:

$$n_i := \sqrt{\left(l_{0,i}\right)^2 + \left(l_{1,i}\right)^2 + \left(l_{2,i}\right)^2}$$

$$ln^{<i>} := \frac{1}{n_i}\cdot l^{<i>}$$

Transformation of l into camera coordinates:

$lln := T \cdot ln$

$$lln = \begin{bmatrix} 0.237 & 0.271 & 0.305 & 0.222 & 0.256 & 0.29 & 0.207 & 0.241 & 0.274 \\ -0.819 & -0.82 & -0.819 & -0.841 & -0.841 & -0.841 & -0.861 & -0.861 & -0.861 \\ -0.522 & -0.504 & -0.486 & -0.494 & -0.476 & -0.458 & -0.465 & -0.448 & -0.429 \end{bmatrix}$$

Drawing lines of possible positions of highlights in the picture:

Gradient of the lines:

$$a_i := \left(\frac{lln_{1,i}}{lln_{0,i}}\right)$$

Calculation of all possible positions:

$$N_{o,p} := \text{wenn}\left[\left[o = \text{runden}\left[a_0 \cdot p + \left(PPexpected_{1,0} - a_0 \cdot PPexpected_{0,0}\right)\right]\right] + o = \text{runden}\ ..., 255, M_{o,p}\right]$$

Drawing white lines in the picture:

$$\text{BMPSCHREIBEN}("c:\text{stillwlin.bmp}") := N$$

Defining the position of the laser end points on the zero levels (still water surface):

$$\Lambda 1_{0,i} := \left(PPexpected_{0,i}\right) \qquad \Lambda 1_{1,i} := \left(PPexpected_{1,i}\right)$$

Calculating the change of the laser end points:

$$\Lambda_i := \sqrt{\left[(\Lambda 2 - \Lambda 1)_{0,i}\right]^2 + \left[(\Lambda 2 - \Lambda 1)_{1,i}\right]^2}$$

Calculating the virtual vector parallel to CCD-chip (equation 3.30-3.33):

$$LL_{1,i} := \frac{-\Lambda_i \cdot MP_i \cdot \left(PP_{1,i} \cdot lln_{2,i} - lln_{1,i} \cdot OO_2 - lln_{1,i} \cdot PP_{2,i}\right)}{\sqrt{\left(PP_{1,i} \cdot lln_{2,i} - lln_{1,i} \cdot OO_2 - lln_{1,i} \cdot PP_{2,i}\right)^2 + \left(lln_{0,i} \cdot OO_2 + lln_{0,i} \cdot PP_{2,i} - PP_{0,i} \cdot lln_{2,i}\right)^2}}$$

$$LL_{0,i} := \sqrt{-\left(LL_{1,i}\right)^2 + \left(\Lambda_i\right)^2 \cdot \left(MP_i\right)^2}$$

$$LL_{2,i} := 0\ \text{m}$$

Transformation of LL into canal coordinate system:

$$L := t \cdot LL$$

Length of laser beams (equation 3.34):

$$\lambda_i := \frac{\left(-L_{1,i} \cdot O_2 - L_{1,i} \cdot P_{2,i} + O_1 \cdot L_{2,i} + P_{1,i} \cdot L_{2,i}\right)}{\left(-ln_{1,i} \cdot O_2 - ln_{1,i} \cdot P_{2,i} - ln_{1,i} \cdot L_{2,i} + ln_{2,i} \cdot O_1 + ln_{2,i} \cdot P_{1,i} + ln_{2,i} \cdot L_{1,i}\right)}$$

The matrix H contains the final result. The second line represents the water height above the points in the measuring plane which coordinates are defined by the first and the third line:

$$H^{\langle i \rangle} := P^{\langle i \rangle} + \lambda_i \cdot ln^{\langle i \rangle}$$

$$H = \begin{bmatrix} 43.215 & 89 & 135.479 & 43.205 & 89 & 135.627 & 43.223 & 89 & 135.732 \\ 177.918 & 172.199 & 159.761 & 177.648 & 168.09 & 155.898 & 178.106 & 172.701 & 153.137 \\ 97.215 & 96.997 & 96.521 & 144 & 144 & 144 & 190.777 & 190.984 & 191.732 \end{bmatrix} \cdot \text{mm}$$

C Graphs of the results

The following nine pictures show the passing of a wave of 40 mm height. The paddle produced waves with a frequency of 1/1.1 Hz. The result appears like a film, recorded with a frequency of 10 Hz. In fact the camera was adjusted to a frequency of 1 Hz because the time difference between the recording of the single pictures is the more exact the lower the frequency of the camera is. At 10 Hz the time period varies about 20 %, at 1 Hz only around 1 %. The following picture sequence contains data of ten succeeding waves. The measurement points are marked with white dots. The photographs already contain the lines of calculated, possible beam end point positions. Beam three in the picture corresponds to the measuring point in the foreground of the graph.

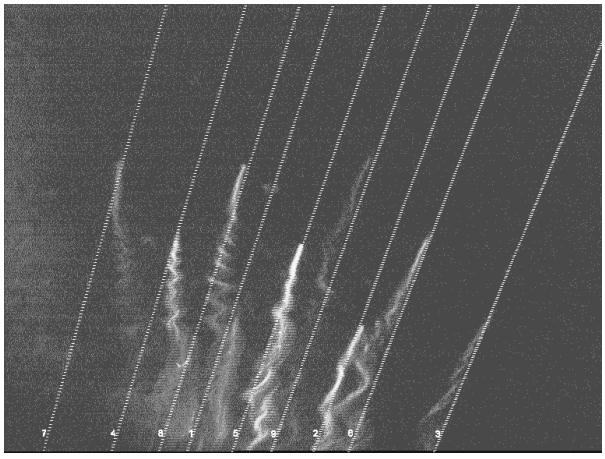

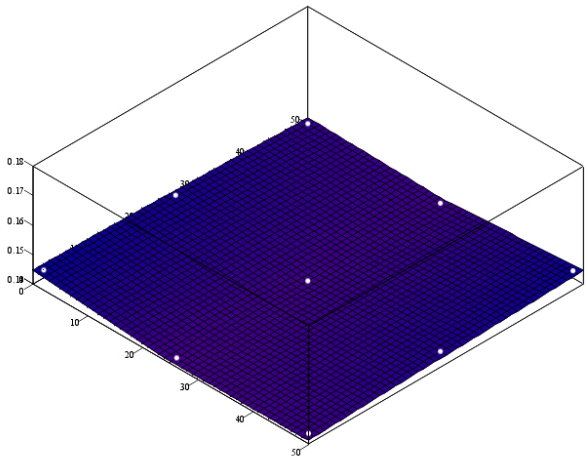

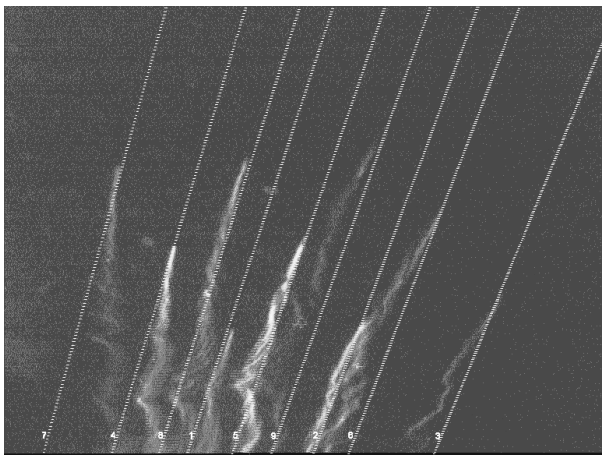

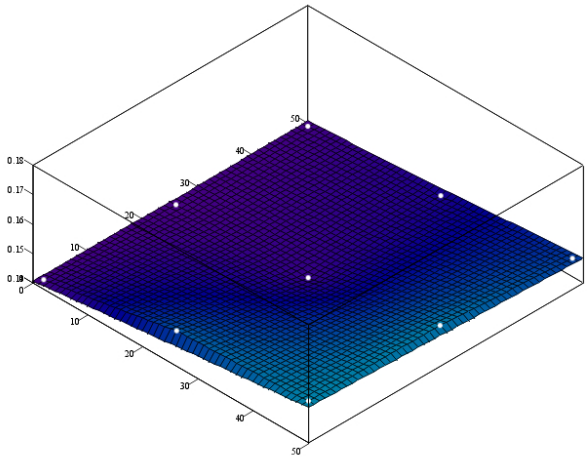

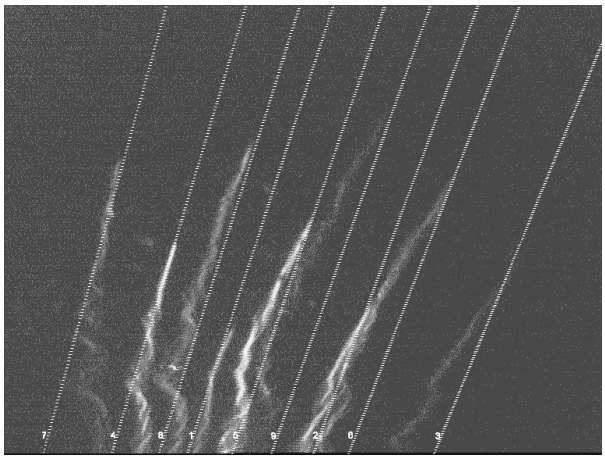

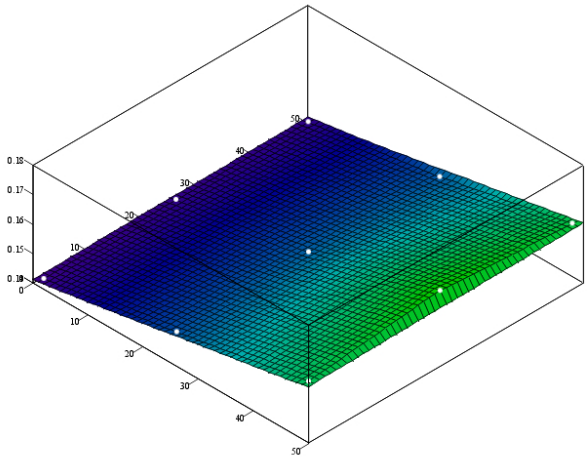

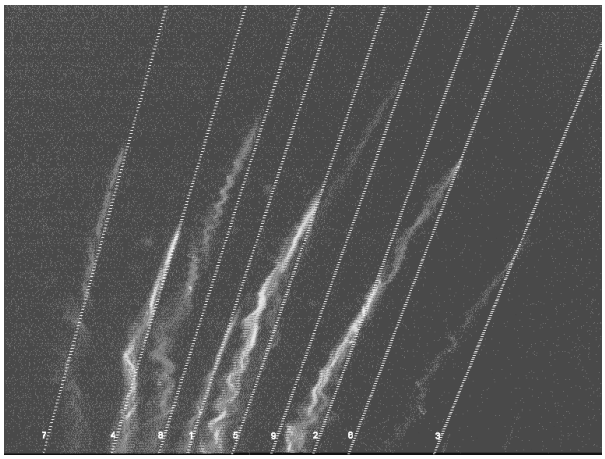

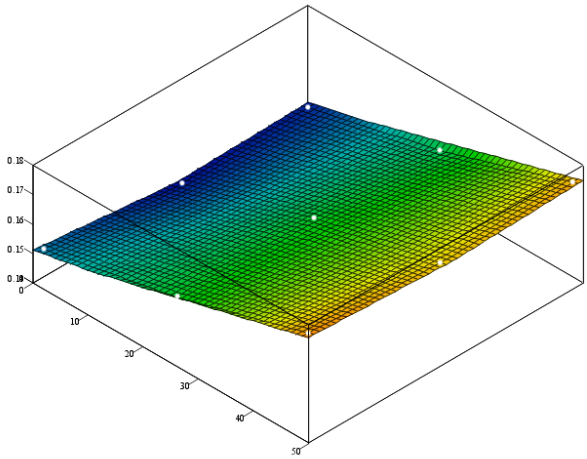

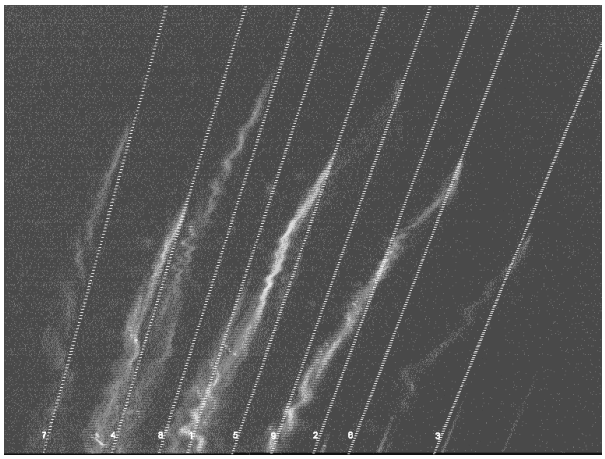

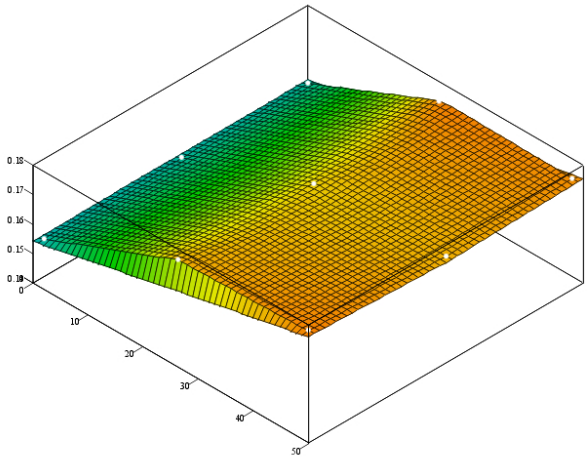

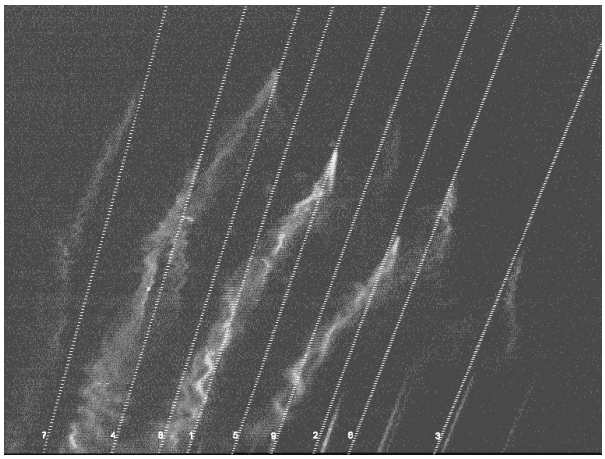

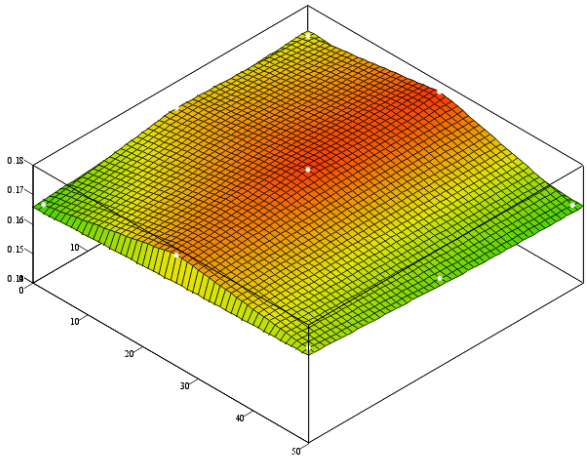

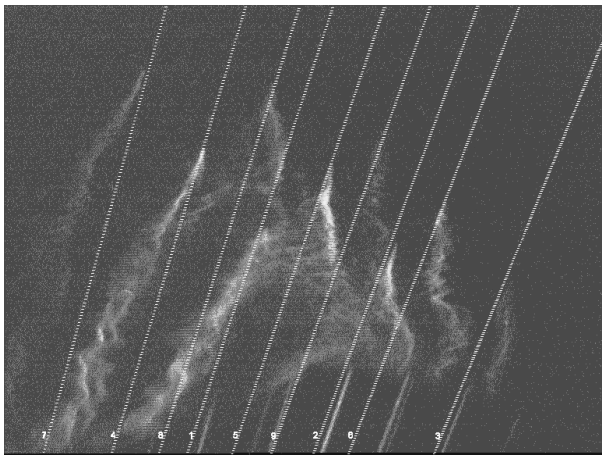

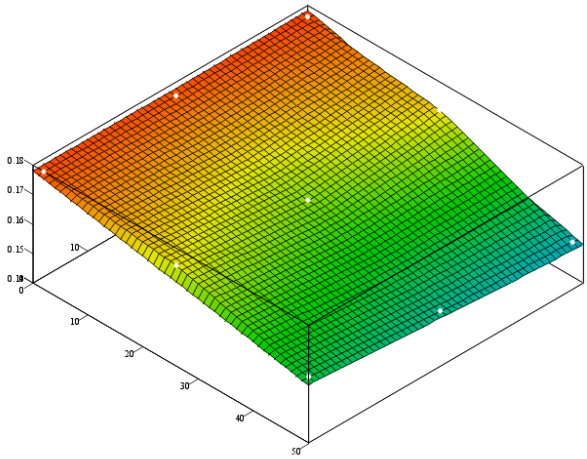

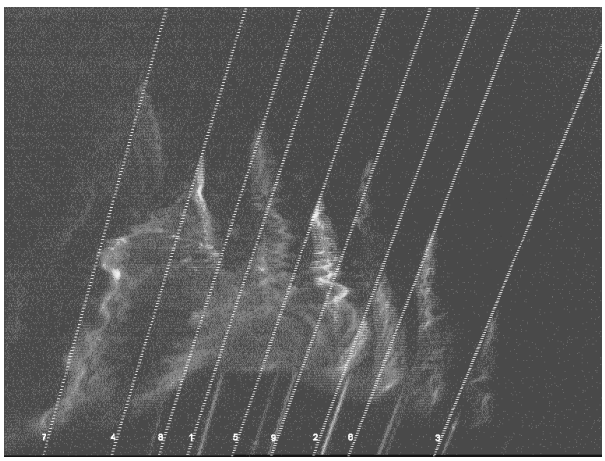

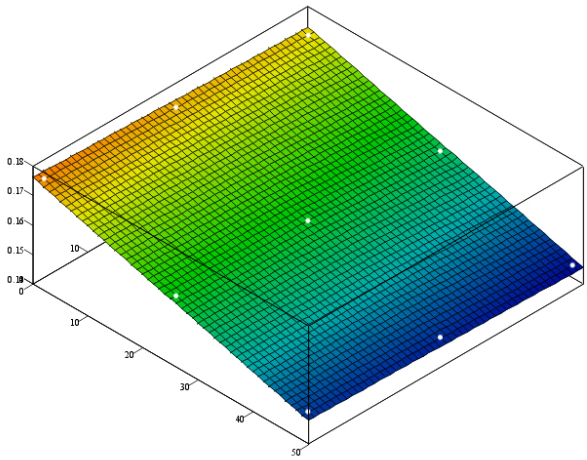

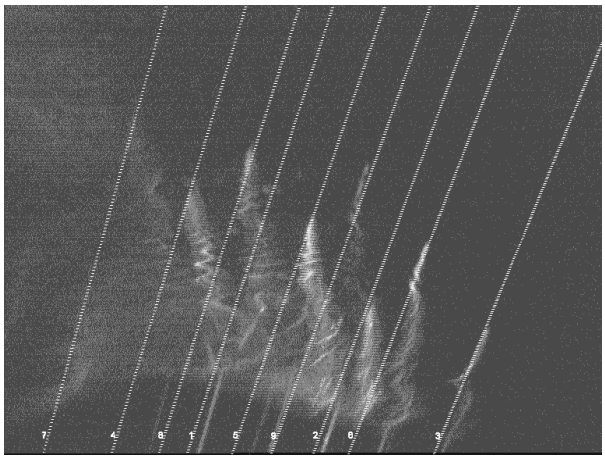

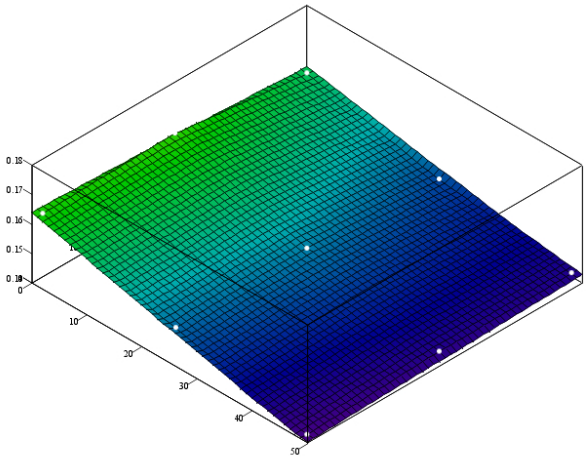
0.18
0.17
0.16
0.15
0
10
20
30
40
50